Article

Integration of Multi-Gas Sensors and Aerial Thermography Into UAVs for Environmental Monitoring of a Landfill

Juan Francisco Escudero-Villegas , Macaria Hernández-Chávez , Bertha Nelly Cabrera-Sánchez , Gilgamesh Luis-Raya , Josué Daniel Rivera-Fernández , Diego A. Fabila-Bustos *

Posted Date: 25 March 2026

doi: 10.20944/preprints202603.1924.v1

Keywords: UAV monitoring; landfill emissions; ordinary kriging

 doi:10.20944/preprints202603.1924.v1

Article

Integration of Multi-Gas Sensors and Aerial Thermography Into UAVs for Environmental Monitoring of a Landfill

Juan Francisco Escudero-Villegas [1], Macaria Hernández-Chávez [1], Bertha Nelly Cabrera-Sánchez [2], Gilgamesh Luis-Raya [3], Josué Daniel Rivera-Fernández [1] and Diego A. Fabila-Bustos [1]*

[1] Laboratorio de Optomecatrónica y Energías, UPIIH, Instituto Politécnico Nacional, Distrito de Educación, Salud, Ciencia, Tecnología e Innovación, San Agustín Tlaxiaca, 42162, Hidalgo, México;

[2] Escuela Superior de Ingeniería y Arquitectura Unidad Tecamachalco, Instituto Politécnico Nacional, Naucalpan de Juárez, 53950, Edo. México, México;

[3] Universidad Politécnica de Pachuca, Carretera Pachuca-Cd. Sahagún km 20 Ex-Hacienda de Santa Bárbara, Zempoala, 43830 Hidalgo, Mexico;

* Correspondence: dfabilab@ipn.mx

Featured Application

The proposed methodology can be applied to the environmental monitoring of landfills by spatially identifying biogas emissions and surface-level thermal anomalies. Its integration into UAV-based monitoring campaigns can assist environmental authorities in detecting critical areas and assessing local variability that is not adequately captured by spot monitoring.

Abstract

Landfills are a significant source of atmospheric emissions associated with the decomposition of organic waste; however, conventional monitoring methods typically have limited spatial coverage. This study evaluated the use of a UAV-based system for the spatial characterization of gases associated with biogas emissions at a municipal landfill. A DJI Matrice 350 RTK platform equipped with a Sniffer4D Mini2 multigass station and a Zenmuse H20T thermal camera was used. Four flight campaigns were conducted at a height of 20 m, with an acquisition frequency of approximately 1 Hz, recording CxHy as an indirect indicator of CH_4, as well as CO_2, CO, NO_2, O_3, SO_2, O_2, temperature, and relative humidity. The results showed a marked transition around 13:10 h, characterized by a simultaneous increase in CH_4 equivalent and CO_2, along with a decrease in NO_2, O_3, and SO_2. Furthermore, CH_4 equivalent and CO_2 exhibited the highest positive correlation among the variables (r = 0.96). The maps obtained using ordinary kriging revealed more heterogeneous patterns, while the qualitative thermal orthophoto confirmed the site's surface variability. Taken together, the results demonstrate that the integration of multigass sensors and aerial thermography on UAVs is viable for the spatial monitoring of landfills.

Keywords: UAV monitoring; landfill emissions; ordinary kriging

1. Introduction

The emission of polluting and greenhouse gases into the atmosphere represents one of the main environmental challenges today, due to its impact on climate change, air quality, and human health. Among the various anthropogenic sources, landfills are a significant source of gas emissions due to the anaerobic degradation of organic waste, a process that generates biogas composed mainly of methane (CH_4) in a proportion ranging from 40% to 70% and carbon dioxide (CO_2) in a proportion ranging from 60% to 30%, along with other trace compounds such as hydrocarbons, carbon monoxide

 doi:10.20944/preprints202603.1924.v1

(CO), nitrogen oxides (NOx), and sulfur dioxide (SO_2) [1, 2]. Methane, for its part, is of paramount importance from a climate perspective, as its global warming potential is much higher than that of CO_2 in the short term, making landfills significant sources of greenhouse gas emissions [3].

The quantification and spatial characterization of these emissions is a fundamental aspect of improving the environmental management of waste disposal sites and developing more efficient mitigation strategies. However, traditional monitoring methods, based on fixed stations or spot measurements on the surface, have significant limitations in terms of spatial coverage and temporal resolution, especially in large or difficult-to-access facilities [4]. In many cases, these types of systems allow reliable time series to be obtained, but they do not adequately capture the spatial variability of emissions or allow for the accurate identification of areas of accumulation or points of biogas leakage. Currently, the development of unmanned aerial vehicles (UAVs) has opened up new opportunities for high-resolution environmental monitoring. These platforms allow atmospheric measurements to be taken in the lower boundary layer with great operational flexibility and the possibility of integrating miniaturized sensors for the detection of multiple gases [5,6].

Various studies have shown that UAVs can be used to obtain vertical gas profiles, track emission plumes, and characterize the spatial distribution of atmospheric pollutants in complex or difficult-to-access environments [7,8]. The reduction in the size and weight of electrochemical, infrared, and spectroscopic sensors has allowed their integration into multirotor platforms, facilitating the simultaneous measurement of compounds such as carbon dioxide (CO_2), methane (CH_4), carbon monoxide (CO), nitrogen dioxide (NO_2), ozone (O3), and sulfur dioxide (SO2) in atmospheric monitoring campaigns [9].

Within this context, one of the most dynamic applications of UAVs is the monitoring of methane emissions at waste management facilities and in the energy sector. Various studies have shown that aerial systems equipped with gas sensors can identify emission points and estimate methane flows using different approaches, including mass balance methods and low-altitude concentration mapping [10,11]. In addition, the use of thermal sensors mounted on UAVs has proven to be a useful tool for identifying thermal anomalies associated with the migration of biogas to the surface, allowing the location of potential leak zones in landfills [12]. These combined approaches improve the identification of emission hot spots and complement conventional monitoring methods. Despite recent advances, most available studies have focused primarily on measuring methane or carbon dioxide, while research that simultaneously integrates the measurement of various atmospheric pollutants associated with biogas is somewhat limited. The integration of multi-gas sensors into UAV platforms represents an opportunity to more comprehensively characterize the dynamics of emissions from landfills and to better understand the interaction between biogas generation processes, local combustion, and atmospheric conditions.

Therefore, the present study aims to evaluate the use of an atmospheric monitoring system based on an unmanned aerial vehicle equipped with a portable multi-gas station for the spatial characterization of gases associated with biogas emissions [11]. To this end, measurement campaigns were carried out using a UAV equipped with an environmental monitoring system capable of recording concentrations of hydrocarbons (CxHy), carbon dioxide (CO_2), carbon monoxide (CO), nitrogen dioxide (NO_2), ozone (O_3), sulfur dioxide (SO_2), oxygen (O_2), as well as meteorological parameters such as temperature and relative humidity. In addition, thermal images were captured using an infrared camera attached to the UAV in order to identify possible thermal anomalies associated with biogas emission processes. Based on this data, spatial distribution maps of gases were generated in order to identify possible accumulation zones and analyze the feasibility of using a combination of UAVs, multi-gas sensors, and aerial thermography as a tool for environmental monitoring of landfills.

2. Materials and Methods

The acquisition of atmospheric data using unmanned aerial vehicles has proven to be a useful alternative for studying the lower atmosphere and for environmental monitoring in locations where

 doi:10.20944/preprints202603.1924.v1

ground access is limited or where the spatial variability of emissions makes it difficult to characterize them using conventional point measurements [4,5]. The integration of miniaturized sensors into these platforms has enabled simultaneous monitoring of different atmospheric variables and trace gases, facilitating the analysis of emissions and their spatial distribution in various environments [6,16].

In the particular case of landfills, this approach is especially relevant due to the heterogeneous nature of gaseous emissions and the need to integrate spatial, thermal, and meteorological information into a single measurement campaign [1,2,12].

This section describes the materials, equipment, and procedures used to acquire and process the data used in this study. First, the study area and its general characteristics are presented, followed by a description of the UAV platform, the multi-gas monitoring system, and the thermal sensor used during the campaign. Finally, the flight planning criteria are detailed, as well as the processing, quality control, and geospatial integration of the data, considering that this type of study requires an adequate association between the position of the UAV, the atmospheric variables measured, and the spatial analysis tools [16,17].

2.1. Study Site

The study was conducted at a municipal solid waste (MSW) disposal site located in central Mexico, east of the State of México. The site has an average altitude of approximately 2,544 m above sea level, which places it within the central Mexican highlands. The area is predominantly mountainous, with variations in altitude that influence local climatic conditions, characterized by a temperate climate and gentle slopes in the area where the disposal site is located.

The landfill operates as a regional infrastructure for the final disposal of municipal solid waste, resulting from an inter-municipal management scheme established with the aim of improving waste management in the region [13]. This operating model was formalized through institutional agreements and subsequently through the creation of a decentralized public body responsible for managing the site [14]. At the institutional level, this type of facility is part of the regional waste management systems recognized in national assessments of infrastructure for urban solid waste management in México [15].

The site mainly receives municipal solid waste from domestic and commercial activities, which is deposited and compacted in final disposal cells. Due to the anaerobic degradation processes of the organic fraction of the waste, biogas is generated, composed mainly of methane (CH_4) and carbon dioxide (CO_2), in addition to other gaseous compounds present in lower concentrations. The site evaluated does not have an active biogas capture or utilization system, which may favor the diffuse release of gases into the atmosphere.

The topographical characteristics of the study area, together with the absence of biogas collection systems and the heterogeneous nature of the landfill surface, can generate complex spatial patterns of gas emissions, including areas of localized biogas accumulation or release. Due to this spatial variability, the site represents a suitable environment for the application of atmospheric monitoring techniques based on unmanned aerial vehicles (UAVs), which allow the spatial distribution of pollutant gases to be characterized.

2.2. UAV Platform

A DJI Matrice 350 RTK unmanned aerial vehicle (UAV) was used to acquire the data. This is an industrial-grade multirotor platform designed for professional environmental monitoring, inspection, and geospatial surveying applications. This type of platform has proven particularly useful in environmental studies due to its flight stability, payload capacity, and ease of integrating multiple sensors for measuring atmospheric and environmental variables [4].

The Matrice 350 RTK incorporates a navigation system based on RTK (Real-Time Kinematic) technology that allows centimeter-level accuracy in the georeferencing of data acquired during flight. This system can provide horizontal accuracies close to 1 cm + 1 ppm and vertical accuracies of 1.5 cm + 1 ppm, facilitating the correct spatial integration of atmospheric measurements obtained during

 doi:10.20944/preprints202603.1924.v1

monitoring campaigns. This type of positioning capability is essential when conducting environmental characterization studies using UAV platforms [5,6]. The platform weighs approximately 6.47 kg, measures 810 x 670 x 430 mm, and has a flight endurance of up to 55 minutes under no-payload conditions. It can also reach a maximum speed of 23 m/s and has a global positioning system compatible with GPS, Galileo, BeiDou, and GLONASS, which improves positioning stability during flight operations. These characteristics make this type of platform suitable for environmental monitoring and high-precision geospatial surveying applications [5].

During the measurement campaigns, the UAV was equipped with two sensing systems. A Sniffer4D Mini2 multi-gas environmental monitoring analyzer, weighing approximately 400 g, was installed on top of the drone to measure various atmospheric pollutants. On the other hand, a DJI Zenmuse H20T thermal camera was incorporated into the bottom of the platform, used to acquire thermal information from the surface of the study site. The flight operations were carried out at an approximate height of 20 m above ground level in order to obtain representative measurements of the gas concentrations and atmospheric conditions present in the study area. A total of four flights were carried out, each lasting approximately 15 minutes. The data generated by the monitoring system were recorded at a temporal frequency close to 1 Hz, determined from the time interval present in the records exported in CSV format, which allowed a continuous time series of the variables monitored during each measurement campaign to be obtained. The main characteristics of the UAV platform used in this study are presented in Table 1.

2.3. Gas Monitoring System

A Sniffer4D Mini2 multi-gas monitoring system, specifically designed for integration into UAV platforms and for real-time environmental data acquisition, was used to measure atmospheric gases during flight campaigns. The use of gas sensors mounted on unmanned aerial vehicles has been widely reported as an effective tool for monitoring fugitive emissions in landfills and other industrial environments, due to their ability to perform measurements with high spatial resolution and detect local variations in gas concentrations [4,6,12].

Table 1. Features and specifications of the UAV platform.

	Specifications
UAV platform	DJI matrice 350 rtk
Weight	6.47 KG
Dimensions	810 × 670 × 430 mm
Autonomy	55 min
Speed	23 m/s
GNSS	GPS + Galileo + BeiDou + GLONASS

The Sniffer4D Mini2 system allows for the simultaneous detection of various gases by integrating different sensing technologies within a single compact module. In this study, the system was configured to measure total hydrocarbons (CxHy), carbon dioxide (CO_2), carbon monoxide (CO), nitrogen dioxide (NO_2), ozone (O_3), sulfur dioxide (SO_2), and oxygen (O_2), as well as to record environmental variables such as temperature and relative humidity, which are relevant for interpreting atmospheric dynamics and pollutant dispersion.

Total hydrocarbons (CxHy) were detected using a sensor based on non-dispersive infrared (NDIR) technology, which makes it possible to quantify the combustible gases present in the biogas produced by the decomposition of organic waste. Due to its stability, selectivity, and ability to detect gases such as methane over relatively wide concentration ranges [7], this type of sensor is frequently used in environmental applications. For the system used, the hydrocarbon measurement range was 0–5% VOL (equivalent to 0–100% of the lower explosive limit, LEL) for methane or 0–2% VOL for

 doi:10.20944/preprints202603.1924.v1

propane, with a theoretical resolution of 0.01%. Measurements of CO, NO_2, SO_2, and O_2 were performed using electrochemical sensors, a technology frequently employed in environmental monitoring due to its high sensitivity for detecting trace gases at relatively low concentrations. In particular, the oxygen measurement module allows for the quantification of concentrations between 0 and 50%, with a detection limit close to 1% and a theoretical resolution below 0.1%. This enables the assessment of changes in atmospheric composition linked to biological and oxidation processes occurring in landfills.

The system also includes a combined O_3 + NO_2 measurement module that uses electrochemical technology and responds simultaneously to both oxidizing compounds. This type of sensor measures the total concentration of atmospheric oxidants, making it possible to calculate the individual concentration of ozone (O_3) by subtracting the amount of NO_2 measured by its own sensor from the total signal (NO_2 + O_3). In this regard, we can calculate the ozone concentration using the following formula:

$$\mathbf{O_3} = (\mathbf{O_3} + \mathbf{NO_2}) - \mathbf{NO_2}, \quad (1)$$

This procedure is standard in environmental monitoring systems that use electrochemical sensors, and it enables the calculation of ozone concentrations in air quality studies and atmospheric monitoring. However, carbon dioxide (CO_2) was measured using NDIR technology, which has a measurement range of up to 50,000 ppm. This allows for the recording of concentration fluctuations related to the organic degradation processes occurring in landfills.

By integrating with the UAV's GNSS system, the system continuously recorded gas concentrations and geographic locations during flights, generating time-series data with geographic references. The data was then exported in CSV format for processing and analysis. This ensured that each concentration measurement was associated with its corresponding spatial location, enabling the creation of gas distribution maps for the study area. The main technical specifications of the gas monitoring system used are presented in Table 2.

Table 2. Technical specifications of the gas monitoring system.

Parameter	Detection method	Range
C_XH_Y/ CH_4/ LEL	non-dispersive infrared (NDIR)	0~5% VOL (0~100% LEL) methane, or 0~2% VOL propane
CO_2	non-dispersive infrared (NDIR)	50000 ppm
CO	electrochemistry	0~1000 ppm
NO_2	electrochemistry	0~11 ppm
O_3 + NO_2	electrochemistry	0~11 ppm
SO_2	electrochemistry	0~100 ppm
O_2	electrochemistry	0 – 50 %

Total hydrocarbons (CxHy) were detected using a sensor based on non-dispersive infrared (NDIR) technology, a technique that enables the quantification of combustible gases in the biogas produced by the decomposition of organic waste. For hydrocarbons, the measurement range in the system used was 0 to 5% VOL (0 to 100% of the lower explosive limit or LEL) for methane or 0 to 2% VOL for propane. The detection limit was close to 0.01% (100 ppm), and the approximate response time was t90 < 30 s.

The CxHy /CH_4/LEL sensor is set by default to measure methane (CH_4), one of the main components of the biogas generated in landfills due to the anaerobic degradation of organic waste. Given this configuration, the CxHy measurements recorded by the system can be understood primarily as an estimate of atmospheric methane concentration, particularly in contexts where this

 doi:10.20944/preprints202603.1924.v1

gas is the major component among the hydrocarbons present. In this study, CxHy concentrations were used as an indirect indicator of the presence of methane, which facilitated the identification of potential areas where biogas could be released or accumulate within the study area.

2.4. Thermal Capture System

To observe temperature fluctuations on the surface of the study area, a thermal camera that operates using infrared radiation is essential. In this project, the thermal camera is used to identify thermal patterns that may be associated with sources of gas emissions or changes in the terrain that are not visible to the naked eye. As noted in the work by Fosco et al. [1], this technology is commonly used to detect sources of pollution and to investigate the environment, specifically in the case of methane emissions from landfills using unmanned aerial vehicles (UAVs) equipped with high-resolution thermal cameras.

The camera selected for this study is the Zenmuse H20T from the UAV system, which combines high-definition thermal imaging with a wide range and the ability to capture accurate temperature data. This camera can generate detailed thermal maps that help detect "hot-spots" or areas with a higher concentration of gases, which is essential for quantifying emissions.

2.5. Planning of UAV Flight Campaigns

Proper planning of flight missions is essential to ensure the quality and reproducibility of data collected by drones, particularly when thermal and gas sensors are incorporated into environmental monitoring studies. According to several authors, photogrammetric accuracy and thermal resolution are directly affected by the precise establishment of routes, flight altitudes, capture modes, and spatial coverage [18]. The measurement campaign was organized following a systematic protocol using DJI Pilot 2 software, which is built into the UAV's remote control. This enabled the safe and effective planning, execution, and monitoring of flights.

2.5.1. Creating the Flight Plan

The flight path tool within the DJI Pilot 2 interface was used to plan the flight campaigns. Next, a georeferenced polygon was drawn to precisely define the area of interest where measurements would be taken. This polygon ensured that the UAV operation remained within safe and permitted limits, while also ensuring uniform coverage during data acquisition.

Once the area had been determined, a grid-based or systematic flight path was automatically generated, allowing the entire defined area to be covered evenly. To ensure a more stable flight and enable representative dispersion of the gases detected by the sensors, various operational and environmental factors were considered during mission planning, particularly the direction and speed of the prevailing wind in the region. In addition, a flight altitude of 20 m above ground level was set to ensure appropriate proximity to the surface without compromising the UAV's operational safety or the quality of the measurements.

The flight path consisted of a series of parallel lines that completely covered the designated area; this method is widely used in environmental monitoring studies involving UAVs, as it ensures that data is evenly distributed throughout the entire area of interest [19]. This flight pattern allows the UAV to perform a systematic sweep, continuously recording gas concentrations. Figure 1 shows an example of the planned flight path, illustrating the operational area and the flight routes taken by the drone to collect data.

 doi:10.20944/preprints202603.1924.v1

Figure 1. Aerial view of the study site. The blue dots indicate the route taken to collect data using a UAV.

2.5.2. Selection of Sensory Configuration and Capture Type

The Matrice 350 RTK aerial platform and the corresponding image capture system were configured after defining the flight polygon. In this case, data acquisition was performed using the optical sensor mounted on the aircraft. Priority was given to capturing high-resolution images for subsequent photogrammetric processing to create georeferenced orthomosaics. The inclusion of the RTK positioning system increased the spatial accuracy of the generated products, thereby reducing uncertainty regarding the location where each image was captured.

An automated flight path with a strictly nadir orientation (90° relative to the ground) was selected to meet the geometric requirements necessary for the production of orthomosaics. This configuration is essential for improving spatial modeling accuracy during photogrammetric processing [20], ensuring adequate longitudinal and lateral overlap between images, and minimizing geometric distortions.

2.5.3. Flight Parameters: Altitude, Speed and Capture Angle

The flight parameters were established in accordance with criteria based on technical recommendations for low-altitude environmental studies [21]. These parameters were chosen to maximize thermal resolution and ensure adequate coverage throughout the entire study area, without compromising the UAV's operational stability.

All the parameters configured for this study—such as flight speed, altitude, and camera angle—are essential for properly acquiring and processing thermal and atmospheric data. They are shown in Table 3.

2.5.4. Mission Execution and Data Recording

The automated mission was carried out after the flight parameters were configured. The UAV followed the predefined route, recording data at regular intervals set by the control software. At the same time, the Sniffer4D Mini2 monitoring station recorded gas concentrations as well as GNSS coordinates. This synchronized operation enabled effective integration of both datasets during geospatial processing and subsequent analysis, ensuring an accurate correlation between the captured imagery and the gas concentration data.

Table 3. UAV flight configuration.

Parameter	Configured value	Description

 doi:10.20944/preprints202603.1924.v1

Flight altitude	20 m AGL	This altitude maximizes thermal resolution without compromising operational safety or the aerodynamic stability of the UAV.
Flight speed	14 m/s	This speed allowed the mission to be completed within the UAV's battery limits while maintaining adequate image overlap for subsequent thermal processing.
Camera angle	90° (nadir)	Automatically adjusted in ortho-collection mode; ensures geometric uniformity, reduces angular variability, and improves photogrammetric reconstruction efficiency.

2.6. Data Processing and Analysis

A data processing and analysis phase was conducted following the completion of the four monitoring campaigns, with the aim of ensuring temporal consistency, comparability among variables, and the reliability of statistical and spatial results. Data were collected at a frequency of 1 Hz during the missions, which enabled a continuous time series of the monitored variables. Subsequently, a database cleaning process was carried out to remove invalid values, inconsistencies, and records that were not suitable for analysis. As a result, a final dataset of 3,600 clean, georeferenced data points was produced, which was used for statistical concentration assessment, exploratory time-series analysis, and spatial preprocessing to create interpolated maps. In general terms, this workflow encompassed database cleaning, standardization of concentration units, exploratory time-series analysis, and spatial preprocessing for the creation of interpolated maps. In environmental studies, this type of procedure is highly recommended, as the quality of the analysis depends largely on the quality and consistency of the input data [22, 23].

2.6.1. Data Preprocessing

To begin with, the original file was reviewed to correct formatting inconsistencies and properly organize the dataset. Specifically, the "Time Stamp" column was corrected by removing residual characters and encoding inconsistencies that prevented it from being properly converted to date and time format. Next, only the variables necessary for the analysis were selected: temperature, relative humidity, SO_2, NO_2, O_3+NO_2, CO_2, CO, O_2, and CxHy/flammable gases. On this occasion, the pressure variable was also included because it was used to perform the necessary conversions for certain parameters. Columns not used in subsequent processing were removed to simplify the organization of the dataset and prevent redundancies. Additionally, the main fields were checked for empty or inconsistent records, in accordance with the general quality control criteria typically applied to environmental and monitoring series [22].

2.6.2. Standardization of Units and Calculation of Variables

Since the gas variables from the monitoring system were originally expressed in different units, it was essential to standardize them in order to express all concentrations in a common unit. To this end, "µg/m³" was used as the standard unit. This decision made it possible to compare and interpret the various chemical species together on the same physical scale, which is particularly beneficial in studies where multiple pollutants are measured simultaneously.

For CO, which was initially reported in mg/m³, a direct conversion to µg/m³ was performed. For O_2 and CxHy, whose readings were recorded as percentages, the conversion was performed using the ideal gas law, taking into account the temperature and pressure measured at each observation and the corresponding molecular weight. For spatial representation and standardization, the CxHy signal was treated as if it were equivalent to methane. This type of adjustment provides a consistent

 doi:10.20944/preprints202603.1924.v1

physical basis for the analysis, particularly when it is necessary to combine variables initially expressed as volume fractions with others reported as mass concentrations.

In addition, the ozone concentration was calculated based on the difference between the combined O_3+NO_2 signal and the standalone NO_2 signal. Therefore, only the combined variable was used as an intermediate input, and the subsequent analysis was performed using the individual concentrations of O_3 and NO_2, as this separation allows for a clearer interpretation of the behavior of each compound.

2.6.3. Time Series and Exploratory Data Analysis

After structuring the database, an exploratory analysis was conducted to identify overall patterns, variations over time, and possible relationships between the variables. Individual time series were generated for each gas, as well as a combined series that facilitated the simultaneous observation of concentration trends throughout the monitoring period. Since some variables exhibited vastly different magnitudes, a scaled representation using z-scores was also developed; this was used solely to facilitate the visual comparison of trends, without ever neglecting the environmental interpretation based on the original concentrations.

Histograms, box plots, and correlation matrices were also generated. Specifically, the correlation map was created using only standardized gas concentrations, while temperature and relative humidity were examined as auxiliary environmental variables. They were therefore considered in the interpretive analysis using scatter plots and separate maps [23]; although these variables are not pollutants in themselves, they can affect the accumulation and dispersion of gases.

2.6.4. Identifying Outliers

Outliers were identified using the interquartile range (IQR) criterion, a commonly used method for identifying observations that deviate significantly from the overall trend of a data series, as part of the quality control process [23]. However, these records were not automatically removed, since in environmental monitoring, concentration spikes are not always instrumental errors; on numerous occasions, they may reflect actual short-term emission events. For this reason, although the outliers were flagged, they remained in the original dataset.

2.6.5. Spatial Processing of Data

To ensure that each record had a valid and consistent location, the original geographic coordinates were validated prior to any interpolation in the spatial phase. The data was then converted to a projected reference system in meters, which enabled proper handling of spatial distances when creating interpolated surfaces. This step is particularly crucial in geospatial methods such as kriging and IDW, as both rely on the spatial relationship between sampling points [24, 25].

The final cartographic products were created using relative local coordinates to avoid publicly disclosing the study site. This made it possible to maintain the validity of the analysis and the spatial geometry of the data without compromising the confidentiality of the actual location of the monitored area.

2.6.6. Spatial Interpolation and Map Generation

To spatially represent the distribution of concentrations, ordinary kriging was applied to the gas variables and as auxiliary environmental variables, to temperature and relative humidity. This method estimates the value at an unsampled location as a weighted linear combination of neighboring observations, according to the following expression:

$$\hat{Z}(x_0) = \sum_{i=1}^{n} \lambda_i Z(x_i) \quad (2)$$

Where:

 doi:10.20944/preprints202603.1924.v1

$\hat{Z}(x_0)$ = is the estimated value at the location x_0.
$Z(x_i)$ = corresponds to the values observed at nearby points.
λ_i = represents the weights assigned to each observation.

In ordinary kriging, these weights are determined based on the spatial dependence structure described by the semivariogram and satisfy the condition of unbiasedness $\sum \lambda_i = 1$. To provide a preliminary visual reference during processing, maps were generated using the Inverse Distance Weighting (IDW) interpolation method. This method offers an initial visual approximation of the spatial pattern of the data and serves as a useful starting point [25]. However, these maps were used only for exploratory purposes and were not included in the final presentation of the results.

Therefore, the maps presented in this study are based solely on ordinary kriging. This method was chosen because of its ability to account for the spatial autocorrelation of the data and to generate more consistent surfaces for environmental analysis [24, 26].

Finally, to preserve the privacy of the study site and ensure visual clarity, the maps were created using relative coordinates, with a uniform design and no direct spatial references.

2.7. Thermal Image Processing and Qualitative Orthophoto Generation

The thermal images obtained during the flight were processed to produce a continuous spatial representation of the surface thermal response of the monitored area. It has been reported that the use of thermal images obtained via UAVs is a useful tool for detecting anomalies on the surface of landfills, as it allows for the identification of areas with different thermal behavior that could be linked to decomposition processes, gas migration, or changes in surface and moisture conditions [27, 31]. However, several authors caution that one must be cautious when interpreting this type of data, as the recorded thermal response also depends on factors such as incident radiation, material emissivity, sensor temperature, and environmental conditions at the time of acquisition [28, 29].

In the initial stage, the images were processed in WebODM, following a general photogrammetric workflow that included importing the images, aligning the available spatial data, reconstructing the scene, and creating a georeferenced thermal orthomosaic. This methodology aligns with the workflows reported for UAV-derived photogrammetric products, in which OpenDroneMap-based tools enable the creation of elevation models, orthomosaics, and other spatial products from aerial images, using an open and reproducible processing environment [28, 30]. The primary product of interest in this research was the thermal orthomosaic, which was used as the basis for the spatial interpretation of the site's surface thermal response.

Next, for cartographic preparation and final visualization, the orthomosaic exported from WebODM was processed in Python. In general terms, this stage involved reading the raster, cropping it to the area to be analyzed, configuring a color scale to highlight spatial contrasts, and producing the final figure using relative coordinates. The goal of this processing was not to recover absolute temperatures, but rather to improve the visual interpretation of the surface's thermal behavior and simplify its comparison with the interpolated gas maps obtained in the study. According to the literature, in the absence of specific corrections for emissivity and environmental conditions or a robust radiometric calibration, the thermal product is more suitable for relative or qualitative analysis than for a strictly quantitative temperature estimate [29, 31].

Consequently, the thermal orthophoto produced in this study was interpreted as a qualitative orthomosaic of relative thermal response, which serves to distinguish areas with higher or lower apparent thermal intensity within the study area. This methodological approach allowed the thermal information to be integrated as a supplementary layer to the gas analysis, without having to assign absolute surface temperature values to the image, which could lead to overinterpretation of the landfill's thermal behavior.

3. Results

In order to provide a comprehensive interpretation of the analyzed area, the results are presented according to various levels of analysis. In the first stage, variations in concentration,

 doi:10.20944/preprints202603.1924.v1

sudden transitions, and patterns that might be common across species were analyzed to understand the temporal behavior of the recorded gases. Next, normalized series, correlation matrices, box plots, and histograms were used to study the dispersion and statistical relationships among the variables. Finally, to identify surface contrasts within the site, ordinary kriging interpolation was used and supplemented with a qualitative thermal orthophoto. Thanks to this sequence, we were able to link the temporal changes in air composition to their spatial expression within the landfill and identify areas that might be affected by processes related to biogas emissions.

3.1. Temporal Behavior of Gas Concentration

The variability over time in the concentrations recorded during the monitoring mission, the sudden changes, the periods of relative stability, and the potential response patterns among the gases were identified through time-series analysis.

An initial phase of CH_4 (Figure 2a) is observed that is relatively stable, with concentrations fluctuating between approximately 145,000 and 180,000 μg/m³. Then, at 13:10 h, a sudden increase is observed, raising the signal to a new level. It experiences fluctuations ranging from approximately 420,000 to 680,000 μg/m³. This change is not the result of an isolated variation, but rather a sustained transition that persists throughout much of the remaining data.

A different pattern can be observed for CO (Figure 2b). At the start of the recording, there is a very sharp peak with values close to 6900 μg/m³, which then drops rapidly to a much more stable range, between 400 and 700 μg/m³. From that point on, the signal shows moderate fluctuations, rather than a sustained increase like the one observed for CH_4.

On the other hand, the CO_2 signal (Figure 2c) reveals one of the most evident patterns throughout the entire campaign. During the first part of the monitoring period, concentrations remained nearly stable at around 382 to 384 μg/m³. However, at 13:10 h, there is a clear jump to a new level of around 515–518 μg/m³. After that transition, the series continues within that range, despite some isolated drops and sporadic peaks. In the case of NO_2 (Figure 2d), the trend is more variable and gradual. The series begins with fairly high concentrations, ranging from 85 to 95 μg/m³, and then gradually decreases to around 30 μg/m³. There is then a partial recovery; however, at 13:10 h, there is another significant drop, with levels falling to less than 20 μg/m³. After this, there is a steady increase until levels reach between 70 and 85 μg/m³. In contrast to CO_2 and CH_4 equivalent, the behavior of NO_2 is less predictable and more gradual than sudden.

O_2 behavior (Figure 2e) should be carefully assessed because its absolute concentration is much higher than that of the other species. Nonetheless, the time series allows for the identification of several relatively unique behavioral patterns throughout the monitoring period. After a noticeable shift in the interval at 13:20 h, the signal shows initial decreases, staggered recovery periods, and a higher and relatively stable level.

The O_3 time series (Figure 2f) shows a highly irregular signal that frequently fluctuates between 60 and 160 μg/m³. Unlike the corresponding CO_2 or CH_4 data, no such marked change is observed; instead, there are points in the middle of the record where relatively higher values and rapid, intermittent drops are recorded, especially around 13:10 h. In contrast, the range of change for SO_2 (Figure 2g) is smaller, approximately between 2 and 14 μg/m³, with mild oscillations throughout the entire period under investigation. Despite not being the main signal among the gases being observed, it exhibits a clear temporal pattern, with an initial progressive reduction, a subsequent recovery, and a notable dip in the interval around 13:10 h.

 doi:10.20944/preprints202603.1924.v1

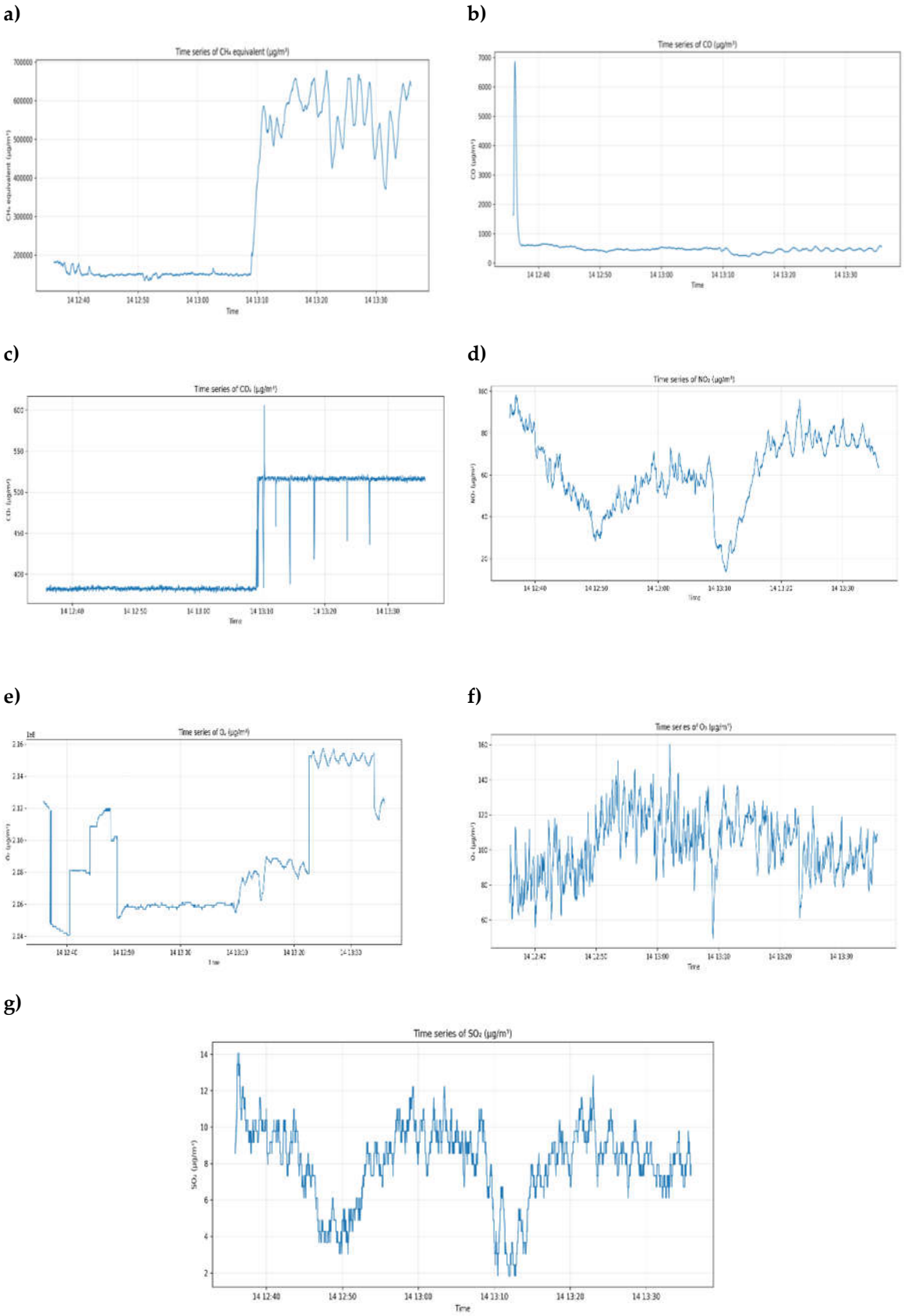

Figure 2. Time series for a) CH_4, b) CO, c) CO_2, d) NO_2, e) O_2, f) O_3, and g) SO_2 during the monitoring mission.

Integrated Analysis of Temporal Variability

To assess their relative fluctuations on a comparable scale, an integrated comparison of gas concentrations was conducted using z-score normalization, in addition to individual analysis of the

 doi:10.20944/preprints202603.1924.v1

time series. This process was necessary because it is difficult to directly compare the monitored parameters in their original units due to differences in order of magnitude between them. Some variables, such as O_2 and CH_4 equivalent, fluctuate within much narrower ranges, while others, such as SO_2, NO_2, and O_3, reach significantly higher levels. In this regard, standardization allowed for a comparison of temporal changes and signal shapes without the absolute magnitude influencing the interpretation.

Each data point is transformed in relation to the mean and standard deviation of its own series as part of Z-score standardization. Each variable is therefore expressed in terms of standard deviations and centered around zero. Consequently, concentrations above the corresponding series' mean are indicated by positive values, and concentrations below that mean are indicated by negative values. As a result, this representation aims to compare the relative intensity of each gas's temporal fluctuations in relation to its own average behavior rather than absolute concentration levels.

Figure 3 shows the combined time series of the normalized variables. Overall, this graph reveals that the monitoring data show a clear transition point at approximately 13:10 h. From that point on, the CH_4 equivalent increases steadily and remains above the average for most of the remaining time. After that same interval, CO_2 shows a similar pattern, with its signal shifting to a relatively higher level.

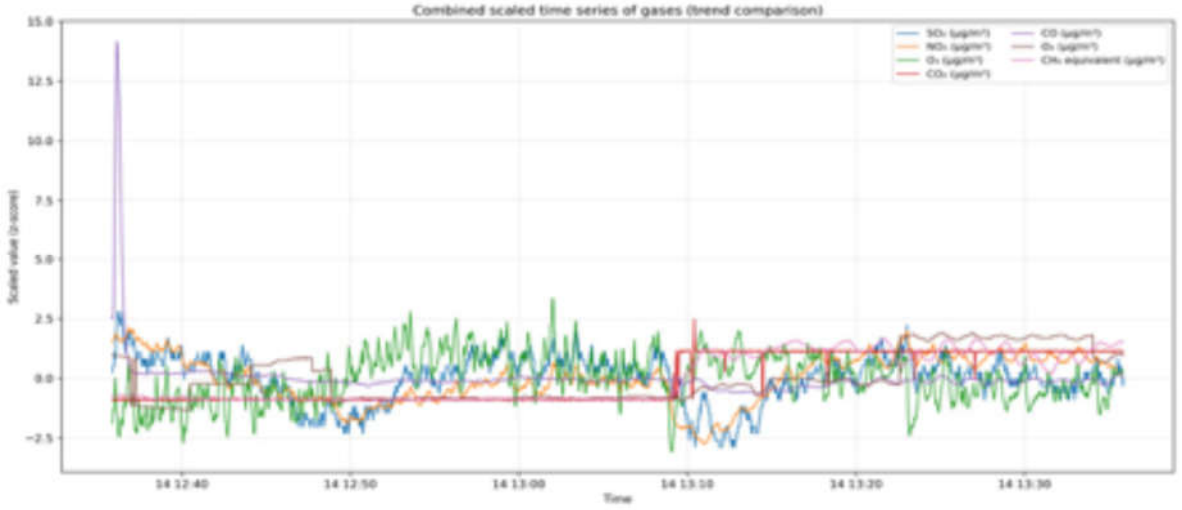

Figure 3. Z-score-normalized time series for comparing trends among the monitored gases.

However, NO_2, SO_2, and O_3 show a decline around 13:10 h, as indicated by the negative z-scores, which reflect concentrations that briefly fall below their mean.

O_2 also shows a change in concentration in the second half of the record, but this should be interpreted with caution due to its high abundance in the atmosphere. CO remains relatively constant throughout the entire record, with the exception of an extreme peak at the beginning that could be considered a one-time occurrence.

3.2. Statical Relationship Between Gaseous Variables

To enhance the visual interpretation derived from the individual time series and the z-score-normalized representation, the statistical relationship between the monitored variables was evaluated using a correlation matrix. This research allowed for the identification of which gases exhibited opposite behaviors, which tended to vary in tandem, and which showed weak or nearly no connections during the monitoring period. The correlation heat map of the measured gas concentrations is displayed in Figure 4.

It's interesting to note that the data showed that CO_2 and CH_4 equivalent had the strongest positive association (r = 0.96). This result is consistent with what was observed in the previous subsections, where both variables increased at roughly 13:10. Significant correlations were also

 doi:10.20944/preprints202603.1924.v1

observed between O_2 and CH_4 equivalent (r = 0.58), CO_2 and O_2 (r = 0.61), and SO_2 and NO_2 (r = 0.72), suggesting that temporal responses were largely shared.

However, the strongest negative correlations were observed between O_3 and O_2 (r = -0.32) and between O3 and NO2 (r = -0.30), suggesting that ozone acted against these variables during a portion of the monitoring period. However, some associations, like those between O_3 and CH_4 equivalent (r = 0.00) and between SO_2 and O_3 (r = -0.02), demonstrated a low temporal correlation.

Analyzing the concentration distribution of each gas over the monitoring period was as important as examining the statistical correlations between the variables. Box plots, which provide a visual depiction of the data's dispersion, central tendency, and outlier occurrence, were used to accomplish this.

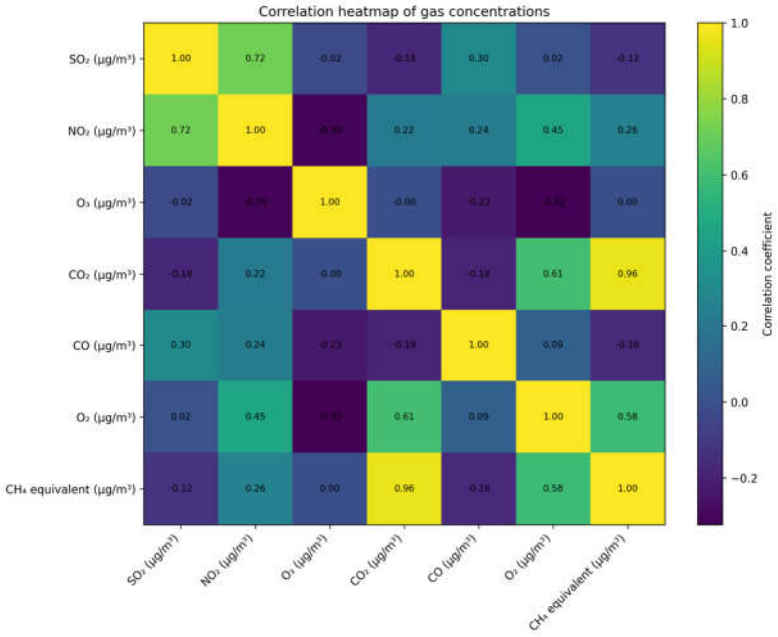

Figure 4. Heat map of the correlation matrix between the concentrations of the gases monitored during the mission.

Distribution and Dispersion of Gas Concentrations

In addition to the temporal analysis and correlation evaluation, box plots of the recorded concentrations for each gas were examined as the data processing progressed. This representation allows for a summary of the data distribution based on the median, the interquartile range, the total range of variation, and the presence of outliers. These elements work together to provide a more complete picture of the dispersion of each variable and the relative stability of its concentrations over time.

The box plots shown in Figure 5 allowed for the identification of outliers in each of the monitored species and a comparative assessment of the recorded concentrations' dispersion. In general, this illustration confirms that the gases exhibited different levels of variability rather than uniform behavior, which is consistent with the patterns previously observed in the correlation analysis and time series.

The CH_4 equivalent and CO_2 examples (Figure 5a-c) show broad distributions, with a large tail extending toward high values and medians pushed toward the lower end of the box. For CO, a different pattern is observed (Figure 5b), where a box plot that is relatively compact coexists with numerous high-magnitude outliers.

On the other hand, the dispersion of NO_2, O_3, and SO_2 showed in Figure 5d-g is moderate or intermediate. NO_2 shows some odd low values, whereas O_3 shows extreme observations at both the bottom and upper ends, suggesting a more variable signal. Few solitary events are also found outside

 doi:10.20944/preprints202603.1924.v1

of the center range, despite the fact that the distribution is more compact in the case of SO_2. When all is said and done, these variables show considerable variability, though not as much as individual CO events or CH_4 equivalent. The behavior of O_2 depicted in Figure 5e also shows a significant amplitude in absolute terms, but it should be interpreted with caution due to its high atmospheric abundance compared to the other species. Nevertheless, the amplitude of the box and whiskers confirmed that this variable also underwent noticeable changes throughout the mission.

a)

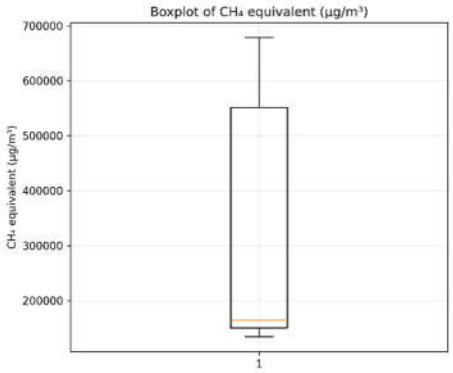

b)

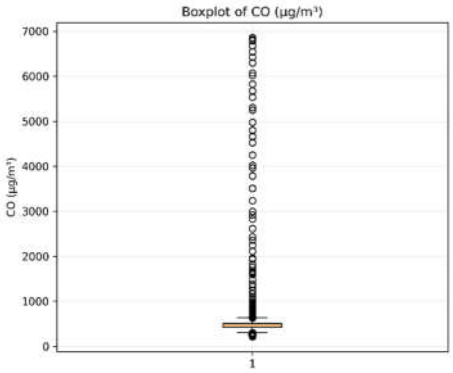

c)

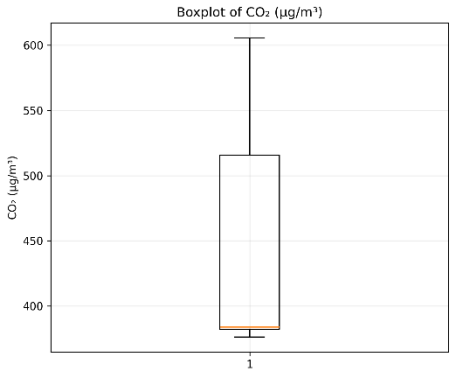

d)

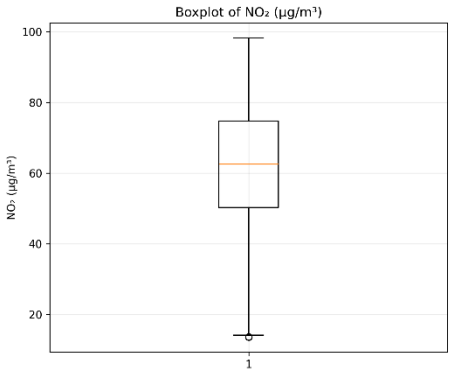

e)

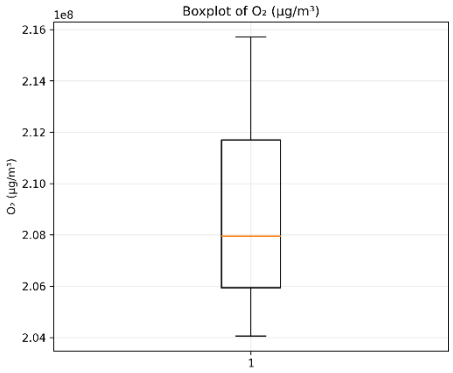

f)

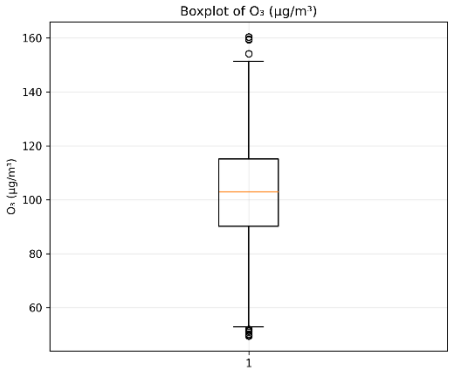

g)

 doi:10.20944/preprints202603.1924.v1

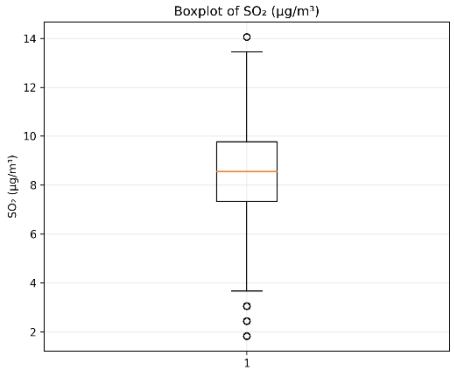

Figure 5. Box plots of the recorded concentrations for (a) CH_4 equivalent, (b) CO, (c) CO_2, (d) NO_2, (e) O_2, (f) O_3, and (g) SO_2, used to compare the dispersion, the central tendency of the data, and the presence of outliers during the monitoring mission.

An alternative interpretation of the data is offered by the histograms in Figure 6, which make it simpler to comprehend which ranges the observations were most frequently concentrated in. Instead of clustering around a single prominent number, the distribution for the CO_2 and CH_4 equivalent measurements (Figure 6a, 6c) shows accumulations at different intervals.

With most of the data concentrated at relatively low values and a smaller fraction extending to significantly higher concentrations, the distribution of the CO histogram (Figure 6b) is clearly biased to the right.

For NO_2, O_3, and SO_2, the distribution is more continuous (Figure 6d, 6f and 6g). O_3 displays a distribution that resembles a wide unimodal curve, centered around intermediate values, whereas NO_2 has a greater range along the concentration axis, indicating significant variability. Conversely, SO_2 concentrates most of its observations into a smaller range, confirming relatively lower dispersion. In the case of O_2, numerous clusters are found across different concentration ranges rather than a single dominant central zone (Figure 6e).

a) **b)**

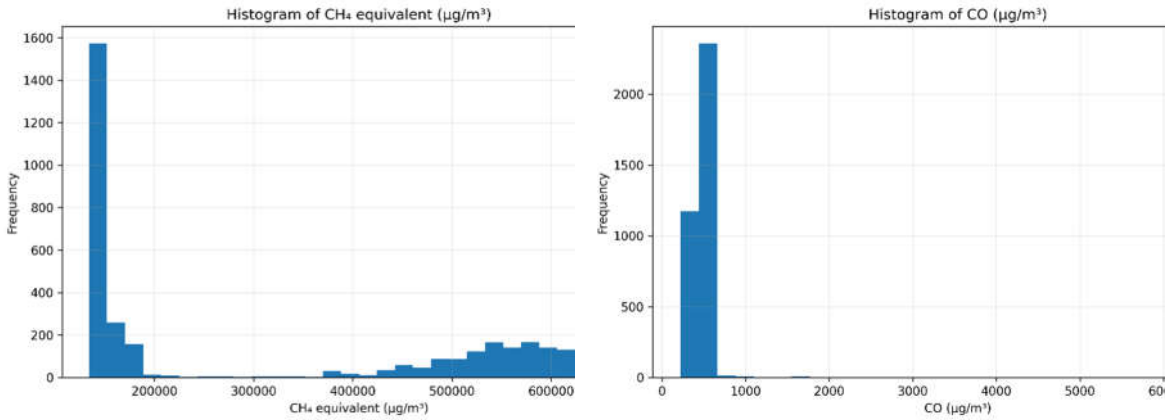

c) **d)**

 doi:10.20944/preprints202603.1924.v1

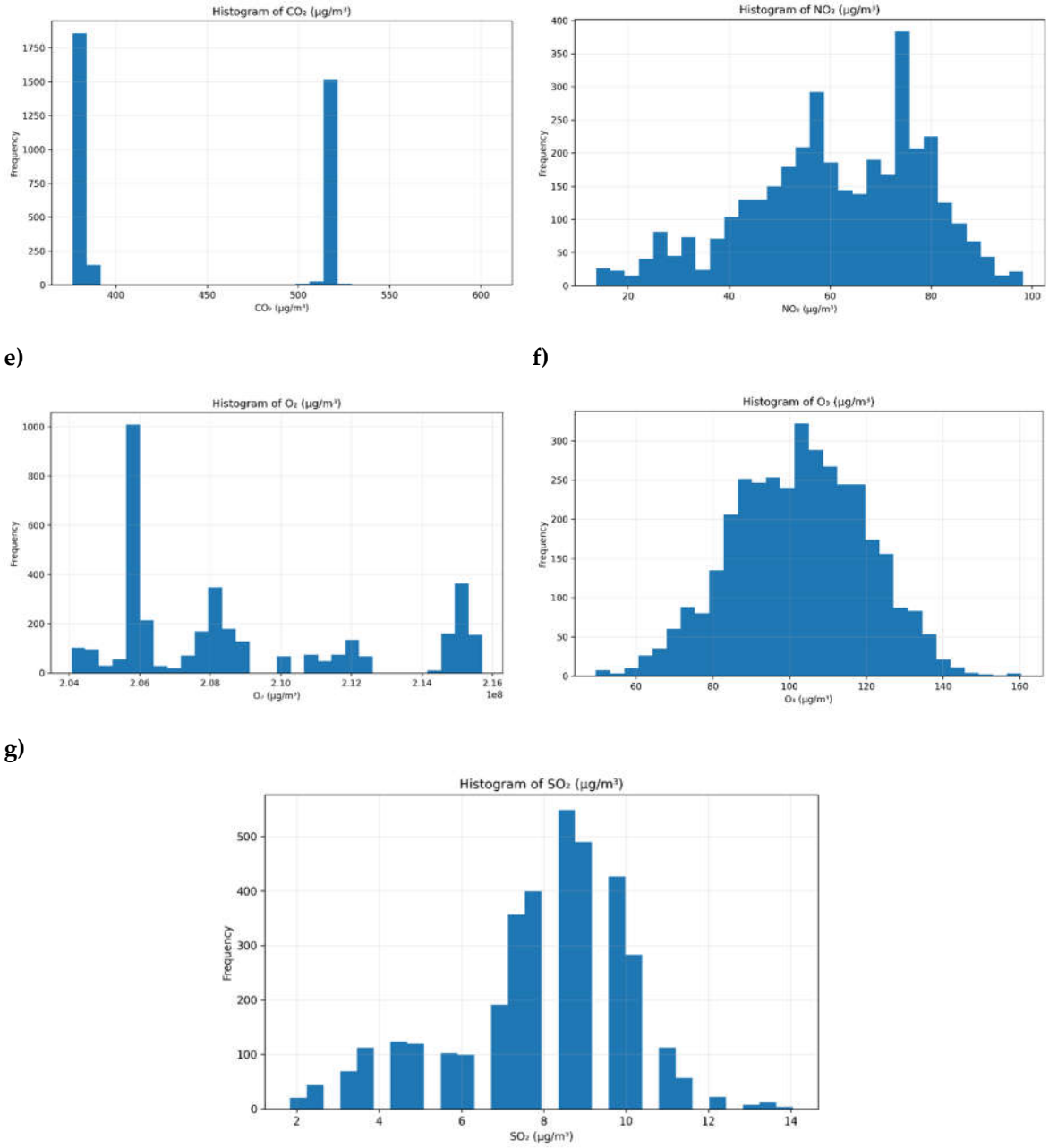

Figure 6. Histograms of the recorded concentrations for a) CH_4 equivalent, b) CO, c) CO_2, d) NO_2, e) O_2, f) O_3, and g) SO_2, used to illustrate the frequency distribution and the predominant concentration ranges during the monitoring mission.

3.3. Spatial Distribution Based on Interpolated Maps

The spatial distribution of the monitored gases within the research area was examined by creating interpolated maps using the standard kriging approach based on the georeferenced data gathered during the measurement surveys. These maps provide a continuous view of concentration fluctuations and facilitate the identification of areas with higher or lower concentrations of each gas. For ease of understanding, the data are presented in pairs of gases, which facilitates the comparison of their spatial patterns.

More noticeable geographic variability can be seen in Figure 7a, which displays the interpolated map of CH_4 equivalent. Higher concentration bands are primarily found in the central, southern, and eastern regions of the monitored area. On the other hand, a minor localized anomaly close to the route's center and areas of lower concentration are found at the western end.Compared to CH_4, the interpolated CO_2 map in Figure 7b shows a more uniform distribution with relatively high and

 doi:10.20944/preprints202603.1924.v1

constant values across most of the studied area. Although there are some isolated areas of lower concentration, particularly in the western sector, in a central anomaly, and toward the northeastern boundary, the interpolated CO_2 surface is generally more uniform and exhibits less abrupt spatial transitions.

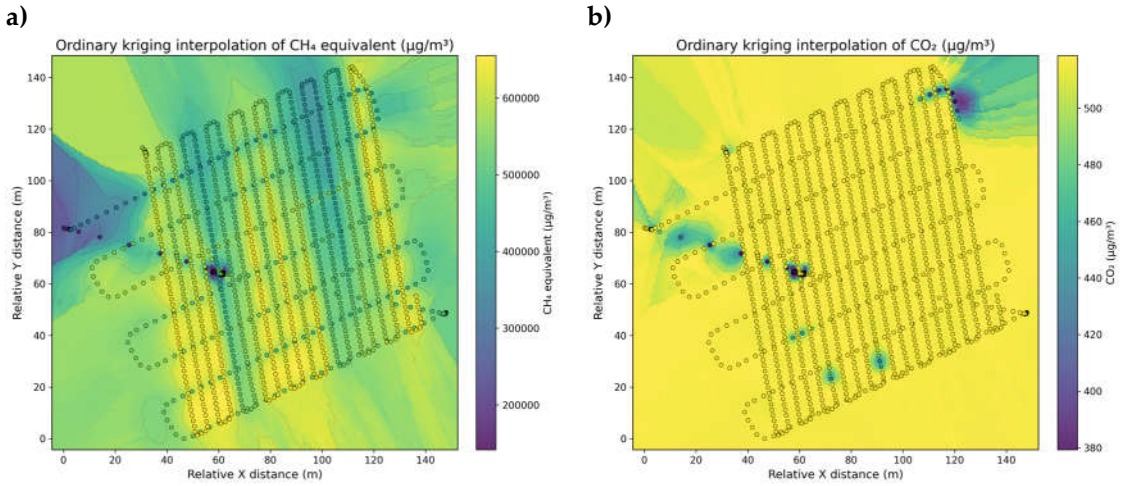

Figure 7. Maps interpolated using ordinary kriging of a) CH_4 equivalent and b) CO_2 in the study area. CH_4 equivalent exhibited greater spatial heterogeneity, while CO_2 showed a relatively more uniform distribution.

Continuing with the map interpolation, Figure 8a, which shows the interpolated O2 map, reveals a fairly wide distribution of high values in the middle of the monitored area, with lower concentrations near its eastern and western borders.

The interpolated CO map in Figure 8b is more varied than the O_2 distribution. Higher-concentration anomalies are visible in the center region and in different parts of the eastern edge, particularly near the intersection of several sampling lines. Concurrently, the lowest concentrations are primarily found near the assessed region's borders, particularly the southwest sector and the eastern boundary.

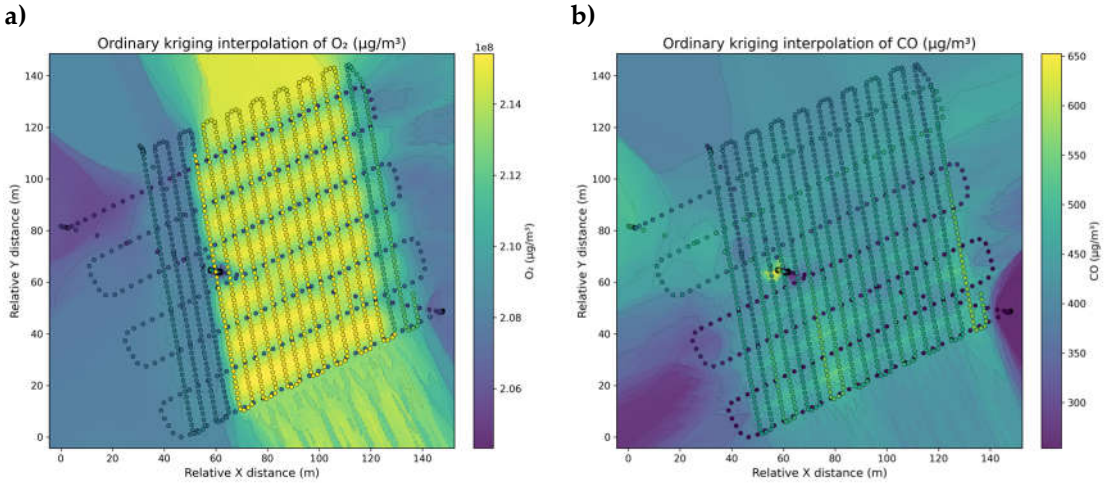

Figure 8. Maps interpolated using ordinary kriging for a) O_2 and b) CO in the study area. O_2 exhibited a relatively more continuous distribution in the central zone, while CO showed greater spatial heterogeneity with localized anomalies.

In contrast, the interpolated NO_2 map in Figure 9a shows a relatively uniform spatial distribution within the main control region, with moderate to high concentrations predominating over a significant portion of the central area. The highest values tend to cluster in bands toward the central and north-central sectors, while the lowest concentrations are most clearly observed at the western and eastern boundaries of the assessed region.

 doi:10.20944/preprints202603.1924.v1

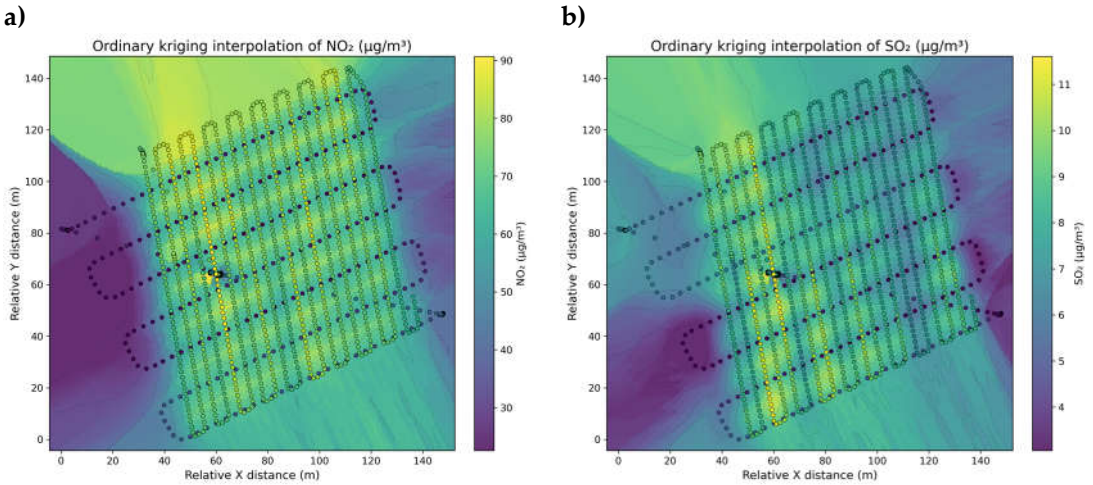

Figure 9. Maps interpolated using ordinary kriging for (a) NO_2 and (b) SO_2 in the study area. NO2 exhibited a relatively more continuous distribution in the central zone, while SO_2 showed a more heterogeneous pattern, with localized anomalies in the central sector.

Additionally, Figure 9b shows a more varied distribution of SO_2, with more isolated abnormalities and more noticeable spatial changes throughout the study area. In this case, the relatively higher concentrations are primarily found in bands in the middle and central-western sectors as well as in some parts of the southern zone, while the lowest values are found along the southwestern edge and in a section of the eastern boundary.

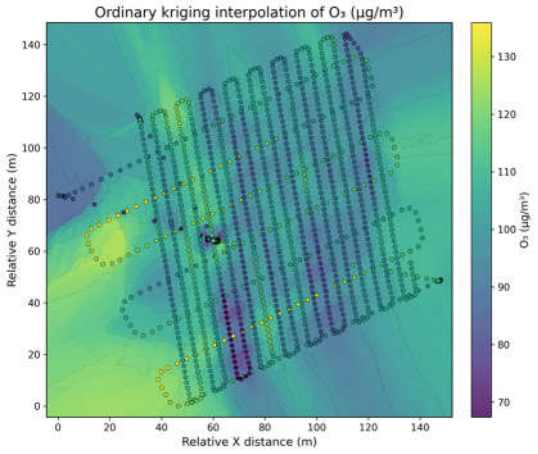

Figure 10. Map of O_3 concentrations in the study area, interpolated using ordinary kriging.

Finally, although it follows a different pattern than the gases that preceded it, the O_3 distribution corresponding to the interpolated map in Figure 10 exhibits a heterogeneous spatial distribution. Comparatively higher concentrations are found in the western and northwestern sectors of the research area, as well as a few remote areas in the southern sector. Conversely, bands of lower concentration are observed within the primary monitoring region, particularly in the central sector and the south-central zone.

3.4. Environmental Variables and Their Relationship to Gas Concentration

In this sense, it is clear from the grouped histograms in Figure 11a, b that both variables displayed distinct ranges of fluctuation throughout the mission, despite having different distributions. In terms of temperature (Figure 11a), the frequency of observations was dispersed across several ranges rather than concentrated in a single interval, suggesting fluctuations in temperature levels throughout the journey. Relative humidity, on the other hand, has a more

 doi:10.20944/preprints202603.1924.v1

continuous distribution (Figure 11b), mainly centered in middle values, but with sufficient amplitude to show environmental fluctuations specific to a site.

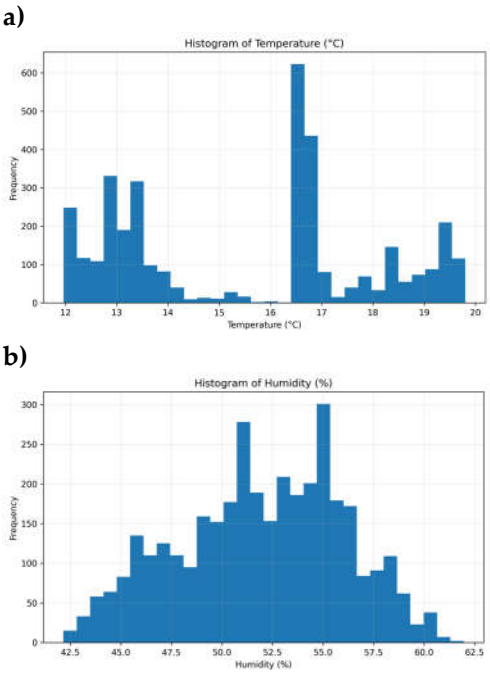

Figure 11. Histograms of (a) temperature and (b) relative humidity, used to visualize the frequency distribution of environmental variables during the monitoring mission.

Temperature and relative humidity were not uniformly distributed throughout the study area, as shown by the interpolated maps in Figure 12a, b. Temperature Figure 12a) shows localized areas with higher values, whereas relative humidity (Figure 12b) shows a varied spatial pattern with sectors where it tends to grow.

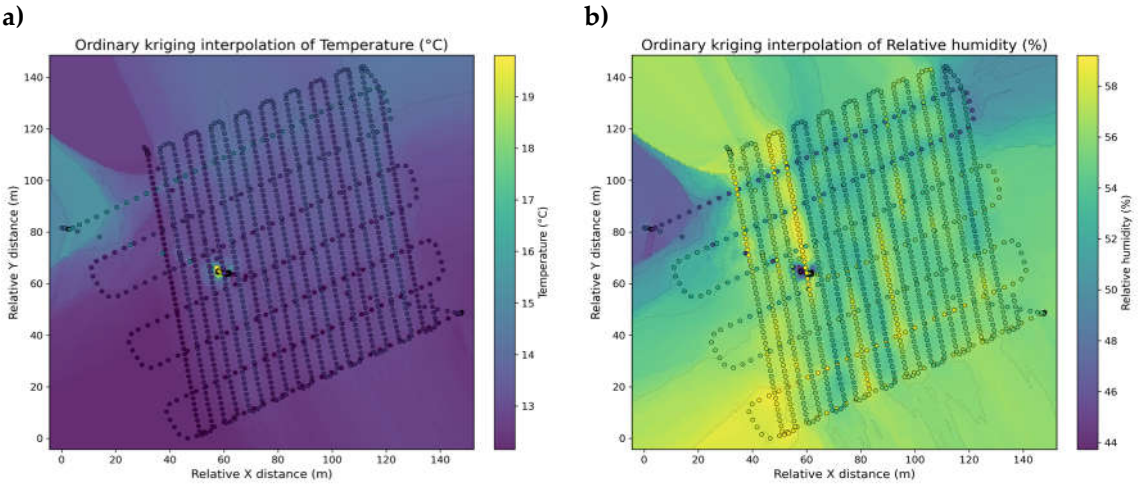

Figure 12. Ordinary kriging interpolation map of environmental variables: (a) temperature, (b) relative humidity, measured at the study site.

Figure 13 provides a more comprehensive view, as it shows a correlation heat map that includes both gases and environmental variables. The most notable correlation is the inverse relationship between CO_2 and temperature (r = -0.91), as well as the one between CH_4 equivalent and temperature (r = -0.91). On the other hand, CO_2 (r = 0.73) and CH_4 equivalent (r = 0.75) have positive correlations with relative humidity.

For the other species, the associations with environmental variables were less pronounced.

 doi:10.20944/preprints202603.1924.v1

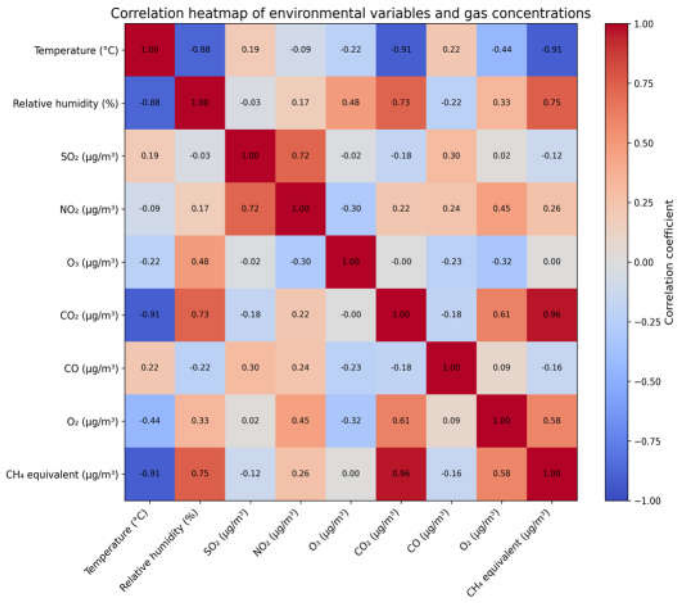

Figure 13. Heat map of the correlation matrix between environmental variables and monitored gas concentrations, used to identify positive, negative, and weak associations between variables.

3.5. Spatial Analysis of the Thermal Orthophoto of the Study Area

To complement the analysis of the interpolated gas maps, a thermal orthophoto of the monitored area was produced using photos taken during the flight and processed using WebODM with Python support for cartographic display. This output allows for the qualitative identification of areas with higher and lower thermal intensity inside the evaluated polygon because it displays a relative thermal response rather than absolute surface temperature data, unlike concentration maps.

Figure 14 shows that the heat response was not uniform across the entire research region. The areas with the highest thermal intensity, represented by colors of yellow and orange, are found in the central, central-eastern, and northern regions of the research area, along with a few linear features associated with highways or exposed surfaces. Conversely, the isolated sections and outer sectors of the site are the areas with the lowest thermal response, which are indicated by dark blue and purple hues. This pattern demonstrates the substantial spatial variation in the landfill's surface thermal signature.

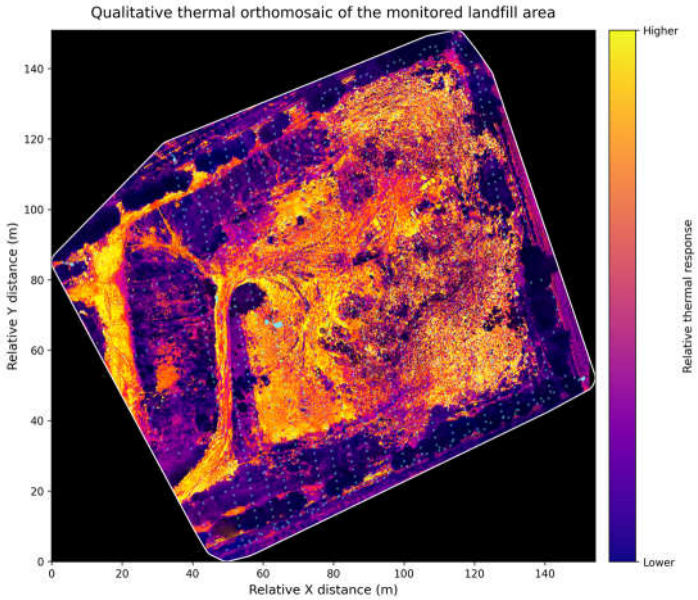

 doi:10.20944/preprints202603.1924.v1

Figure 14. Qualitative thermal orthophoto of the monitored area at the landfill. The color scale represents the relative thermal response of the surface, ranging from areas of lower to higher apparent thermal intensity, without indicating absolute temperature values.

4. Discussion

This sequence allowed us to relate temporal changes in air composition to their spatial expression within the landfill and to identify sectors potentially influenced by processes associated with biogas emissions.

4.1. Temporal Behavior of Gas Concentration

Because each gas has its own concentration ranges and variation mechanisms, individual examination of the time series was necessary to identify emission patterns, local accumulation, and potential effects of atmospheric dispersion along the path. Interpretively, this tendency suggests that the monitoring equipment passed through an area with greater methane concentrations or where atmospheric circumstances promoted local methane storage.

This suggests that CO was likely affected by a point source at the start or by transient conditions different from those that governed methane behavior because it did not respond to the change observed halfway through the monitoring period in the same way.

The temporal congruence between the abrupt increase in CH_4 equivalent and the virtually simultaneous change in behavior of both gases is particularly noteworthy. This lends credence to the theory that the system entered a region with a different gas composition or that site-associated emissions had a bigger effect there. This may indicate that its concentration was more influenced by background sources outside the study location, atmospheric mixing processes, or local ventilation.

Although it may be anticipated that higher concentrations of gases associated with degradation processes would result in a more pronounced decrease in oxygen, this relationship does not manifest itself here in a clear-cut or instantaneous manner. This is explained by the great atmospheric abundance of O_2 and the fact that its relative changes are far less obvious than those of other trace gases. This unpredictability was expected because ozone is a secondary pollutant whose dynamics are mostly dependent on photochemical reactions and air mixing conditions. As a result, its signal appears to respond more to the immediate air environment than to a limited direct emission.

This decline's temporal congruence with the shift seen in other variables indicates that SO_2 responded to the change in the measured air's conditions, albeit at a relatively lower intensity.

When taken as a whole, the time series indicates that the mission underwent a significant turning point at around 13:10 h. At that moment, CO_2 and CH_4 equivalent drastically increased while NO_2, O_3, and SO_2 significantly declined. This synchrony indicates a significant change in the composition of the tested air, which could be caused by approaching an area that is more heavily affected by site emissions, has different ventilation, or has conditions that are more favorable for the local concentration of specific gases. Although the time series do not allow us to pinpoint the exact reason of this change, they show consistent behavior that is apparent concurrently across multiple species.

Integrated Analysis of Temporal Variability

The temporal coincidence between both variables, which suggests that the monitoring equipment reached an area with a different gas composition or with a stronger influence from local emissions, supports the previous conclusion based on the separate time series. This behavior shows that distinct atmospheric processes influenced separate variables instead of all responding in accordance with the same dynamics, which is the opposite of what was observed for CO_2 and CH_4 equivalent.

In general, it can be observed (see Figure 3) that at approximately 13:10 h, there was a substantial change in the composition of the analyzed air, as evidenced by the simultaneous, albeit divergent, reactions of the various gaseous species.

 doi:10.20944/preprints202603.1924.v1

4.2. Statistical Relationship Between Gaseous Variables

Overall, the results indicate contradictory correlations between variables, indicating that the dynamics of the system were governed by a combination of emission processes, local accumulation, and atmospheric mixing rather than by a single behavioral pattern.

These results demonstrate that while the reactions of the other species varied considerably, the dynamics of CO_2 and CH_4 equivalent were relatively comparable. This suggests that the composition of the air under observation was influenced by a number of variables rather than a single, reliable source. As a result, the correlation analysis provides a useful quantitative basis for verifying the presence of both similar and distinct behaviors among gases, strengthening the comprehensive interpretation of the temporal data.

Distribution and Dispersion of Gas Concentrations

The regime change that was observed at around 13:10 hours is consistent with this trend, which indicates a notable shift in concentration levels. Thus, the breadth of both distributions supports the hypothesis that at least two distinct air composition states coexisted during the monitoring period. This implies that even though most of the data were concentrated within a reasonable range, there were sporadic events with concentrations much higher than the core trend of the series. In this way, CO appears to have been dominated by short-lived events rather than a consistent increase throughout the study.

In general, the variables under observation displayed distinct dynamics: species such as NO_2, O_3, and SO_2 exhibit more moderate fluctuations, albeit with sporadic deviations from the usual pattern; while CH_4 equivalent and CO_2 reflect well-defined regime shifts, CO stands out due to the presence of multiple outliers. These results complement the previous temporal study and provide a better picture of the dispersion and relative stability of each gas during the monitoring period.

This separation between the groups supports the hypothesis that both gases underwent a significant change in their concentration levels, which is consistent with the results of the time-series analysis. Consequently, the shape of the distribution lends credence to the idea that the overall behavior of CO was relatively stable, albeit punctuated by large-scale exceptional events.

This implies that the variable's level fluctuated during the mission, but once more its interpretation needs to be done carefully because of the species' characteristics within the atmospheric composition.

Finally, (see Figures 5a–g and 6a–g) show that the observed variables exhibited different distribution patterns. Species such as NO_2, O_3, and SO_2 display more stable and moderate behavior, whereas CO_2 and the CH_4 equivalent show significant variations at different concentrations. The occurrence of sporadic extreme events makes CO unique. These statistical data support the interpretation presented in the previous subsections and confirm that the variability observed during the monitoring period was due to distinct dynamics among the gases.

4.3. Spatial Distribution Based on Interpolated Maps

This pattern suggests that methane was not distributed uniformly throughout the site (see Figure 7), but rather exhibited a more localized distribution, most likely as a result of preferential emission points or differences in the intensity of the landfill's decomposition processes. Increased atmospheric mixing and the fact that CO_2 is affected by the background concentration of ambient air, in addition to its possible contribution from waste degradation, could be related to this behavior.

When the two maps are compared, it can be seen that the CH_4 equivalent was better at revealing spatial variability within the monitored area, while CO_2 showed a more diffuse and stable signal. Interestingly, some areas of lower concentration appear to coincide for both gases, particularly in the western sector and a small center region. This could be caused by local ventilation systems, atmospheric dilution, or a decreased direct impact from active emission sources.

 doi:10.20944/preprints202603.1924.v1

This pattern indicated that oxygen had a moderate geographical variance and a more continuous signal within the primary sampling polygon. Combining the two images suggests that while O_2 maintained a more continuous distribution within the site, CO displayed more distinct and confined spatial fluctuations (see Figure 8).

In the case of NO_2, the pattern showed moderate variability, with a less fragmented distribution than that of other gases and a spatial gradient that decreases toward the site boundaries. However, in the case of SO_2, the spatial pattern appears to be more concentrated, with more distinct areas of higher concentration (see Figure 9). A combination of these data reveals that, although the concentrations of both gases in the central area of the site are similar, NO_2 exhibited a more widespread and continuous pattern, whereas SO_2 made it easier to distinguish isolated areas of variation.

This pattern implies that ozone (O_3) showed a more erratic distribution with more noticeable spatial changes, which may be related to local atmospheric transformation, mixing, and transport processes within the research area.

4.4. Environmental Variables and Their Relationship to Gas Concentrations

In addition to the study of gaseous species, temperature and relative humidity were taken into consideration as supporting environmental variables since both could influence local dispersion and accumulation conditions within the monitored area. Their inclusion allowed for a more comprehensive interpretation of the patterns observed in the gases, particularly when significant statistical correlations and regime transitions were discovered.

This variation in distribution suggests the existence of microenvironments within the study area, which is key to understanding the observed fluctuations in gas concentrations. Taken together, these results (see Figures 11, 12, and 13) show that higher concentrations of both gases tended to coincide with lower temperatures and higher relative humidity during the study period.

Relative humidity showed a moderately strong correlation with O_3 ($r = 0.48$), while temperature showed little correlation with SO_2, NO_2, O_3, and CO (see Figure 13). This suggests that the effects of environmental factors were not the same for all species but were more apparent in those that also displayed shared temporal dynamics, as was the case with CO_2 and CH_4 equivalent.

The addition of temperature and relative humidity provides a useful environmental context for examining the temporal and spatial behavior of the gases being observed. Although these relationships should be interpreted as associations rather than evidence of direct causation, the results suggest that the site's microenvironmental conditions may have favored the local accumulation of particular species during the mission, suggesting that environmental variations are in fact important parameters when monitoring the spatial distribution of gases.

4.5. Spatial Analysis of the Thermal Orthophoto of the Study Area

Generally speaking, variations in the terrain's surface properties, such as the amount of solar exposure, the existence of exposed materials, surface moisture, vegetation cover, and the heterogeneity of the waste that has been deposited may be linked to the observed differences. In this sense, areas with lower thermal intensity may be affected by shade, moisture, or vegetation, whereas areas with higher thermal response may be linked to drier, more compacted surfaces or those with less coverage (see Figure 14). However, these contrasts should be understood as relative thermal patterns rather than as a precise measurement of absolute temperature because the orthophoto is qualitative in nature.

Thermal orthophotos provide a spatial perspective that improves gas monitoring by making it possible to identify areas within the site with distinct surface behavior. Although this product does not by itself allow the establishment of a direct link to internal landfill processes or to specific emissions, it is a useful tool for identifying surface anomalies and supporting a thorough interpretation of the environmental conditions observed during the measurement campaign.

 doi:10.20944/preprints202603.1924.v1

In the end, the results suggest that there was considerable geographical heterogeneity in the monitored area for both the gas distribution and the surface heat response. The interpolated maps allowed us to identify differences in the spatial behavior of each gas. Compounds such as CO, SO_2, and CH_4 equivalent showed more heterogeneous patterns, but CO_2, O_2, and NO_2 showed relatively more consistent distributions within the research area. Furthermore, the qualitative thermal orthophoto confirmed the presence of zones with different apparent thermal intensities, supporting the notion that the site's surface conditions are not uniform. In this way, the integration of the generated geospatial products provided a more comprehensive understanding of the landfill's environmental behavior, offering a useful basis for identifying regions of interest and for future studies intended to evaluate emissions and surface abnormalities.

5. Conclusions

This work demonstrated the feasibility of using a UAV-based atmospheric monitoring system for the geographic characterization of gases associated with biogas emissions at a landfill. The integration of a multi-gas station with a thermal camera installed on a DJI Matrice 350 RTK platform allowed for the collection of georeferenced data with sufficient detail to investigate the temporal behavior, statistical correlations between variables, and spatial distribution patterns of the compounds under observation. The proposed methodology provides a flexible and useful alternative for environmental assessment of sites where traditional point monitoring is insufficient to capture local variability.

The results showed that the air's composition altered throughout the flight. There was a discernible change around 13:10 h that suggested arrival into a region with a different air composition and greater impact from nearby pollutants. At that moment, NO_2, O_3, and SO_2 decreased while CH_4 equivalent and CO_2 increased concurrently. This view was corroborated by the dataset's greatest positive correlation between CO_2 and CH_4 equivalent (r = 0.96), which showed that both variables had closely connected temporal dynamics throughout the campaign.

From a spatial perspective, the interpolated maps showed that, while CH_4 equivalent, CO, and SO_2 displayed more varied patterns, CO_2, O_2, and NO_2 tended to display relatively more continuous distributions within the monitored region. On the other hand, O_3 displayed a more unpredictable spatial pattern consistent with the effects of local mixing, transport, and atmospheric transformation. Furthermore, as evidenced by positive correlations with relative humidity (r = 0.75 and r = 0.73, respectively) and negative correlations with temperature (r = -0.91), higher concentrations of CO_2 and CH_4 equivalent tended to be associated with higher relative humidity and lower temperatures.

Additionally, the qualitative thermal orthophoto confirmed that the landfill's surface showed clear variations in relative temperature responsiveness rather than uniform conditions, particularly in the central, central-eastern, and northern regions of the site. Although it does not allow the inference of absolute temperatures or the development of a direct relationship with internal landfill processes on its own, this product offered helpful spatial context and supported the interpretation of surface heterogeneity seen in the gas maps. Thus, the combination of multi-gas monitoring, geostatistical interpolation, and qualitative aerial thermography can create a more complete picture of the environmental behavior of the evaluated area. Further work should include multi-temporal campaigns, additional meteorological controls, and thermal processing with radiometric calibration to strengthen the interpretation of emission dynamics and improve the site's environmental diagnostic.

Author Contributions: Conceptualization, M.H.-C., G.L.-R. and D.A.F.-B.; methodology, J.F.E.-V., B.N.C.-S., M.H.-C. and J.D.R.-F.; software, J.F.E.-V., J.D.R.-F. and G.L.-R.; validation, J.F.E.-V., J.D.R.-F., M.H.-C., G.L.-R. and D.A.F.-B.; formal analysis, J.F.E.-V. and J.D.R.-F.; investigation, J.F.E.-V., J.D.R.-F., M.H.-C., G.L.-R. and D.A.F.-B.; resources, M.H.-C., G.L.-R. and D.A.F.-B.; data curation, J.F.E.-V., J.D.R.-F. and G.L.-R.; writing—original draft preparation, J.F.E.-V., J.D.R.-F., M.H.-C. and D.A.F.-B.; writing—review and editing, J.F.E.-V.,

 doi:10.20944/preprints202603.1924.v1

M.H.-C. and D.A.F.-B.; visualization, J.F.E.-V., B.N.C.-S., M.H.-C., J.D.R.-F.; supervision, M.H.-C. and D.A.F.-B.; project administration, D.A.F.-B.; funding acquisition, D.A.F.-B.

Funding: This research was supported by the Secretaría de Educación, Ciencia, Tecnología e Innovacion (SECTEI) of CDMX through the Project "Mapeo y cuantificación CH_4, CO, CO_2, NOx y SOx en suelo y aire de la CDMX como estrategia de mitigación de gases para la reducción de efectos del cambio climático", SECTEI/083/2024 awarded to Diego Adrián Fabila Bustos. Juan Francisco Escudero Villegas has scholarship from SIP–IPN through the Programa de Maestría en Ingeniería y Diseño de Sistemas Sostenibles at IPN.

Institutional Review Board Statement: Not applicable.

Informed Consent Statement: Not applicable.

Data Availability Statement: Data presented in this study are available on request from the corresponding author.

Acknowledgments: The authors would like to thank the public institution that provided the facilities for conducting this study at the landfill, as well as for granting access to the monitoring site. The comments and suggestions by the reviewers are deeply appreciated.

Conflicts of Interest: The authors declare no conflicts of interest.

References

1. Fosco, D.; Molfetta, M.D.; Renzulli, P.; Notarnicola, B.; Carella, C.; Fedele, G. Innovative Drone-Based Methodology for Quantifying Methane Emissions from Landfills. *Waste Management* **2025**, *195*, 79-91, doi:10.1016/j.wasman.2025.01.033.
2. Fjelsted, L.; Christensen, A.G.; Larsen, J.E.; Kjeldsen, P.; Scheutz, C. Assessment of a Landfill Methane Emission Screening Method Using an Unmanned Aerial Vehicle Mounted Thermal Infrared Camera – A Field Study. *Waste Management* **2018**, *87*, 893-904, doi:10.1016/j.wasman.2018.05.031.
3. Johnson, D.; Clark, N.; Heltzel, R.; Darzi, M.; Footer, T.L.; Herndon, S.; Thoma, E.D. Methane Emissions from Oil and Gas Production Sites and Their Storage Tanks in West Virginia. *Atmospheric Environment X* **2022**, *16*, 100193, doi:10.1016/j.aeaoa.2022.100193.
4. Alvear, O.; Zema, N.R.; Natalizio, E.; Calafate, C.T. Using UAV-Based Systems to Monitor Air Pollution in Areas with Poor Accessibility. *Journal Of Advanced Transportation* **2017**, *2017*, 1-14, doi:10.1155/2017/8204353.
5. Villa, T.; Gonzalez, F.; Miljievic, B.; Ristovski, Z.; Morawska, L. An Overview of Small Unmanned Aerial Vehicles for Air Quality Measurements: Present Applications and Future Prospectives. *Sensors* **2016**, *16*, 1072, doi:10.3390/s16071072.
6. Burgués, J.; Marco, S. Environmental Chemical Sensing Using Small Drones: A Review. *The Science Of The Total Environment* **2020**, *748*, 141172, doi:10.1016/j.scitotenv.2020.141172.
7. Berman, E.S.F.; Fladeland, M.; Liem, J.; Kolyer, R.; Gupta, M. Greenhouse Gas Analyzer for Measurements of Carbon Dioxide, Methane, and Water Vapor Aboard an Unmanned Aerial Vehicle. *Sensors And Actuators B Chemical* **2012**, *169*, 128-135, doi:10.1016/j.snb.2012.04.036.
8. Greatwood, C.; Richardson, T.; Freer, J.; Thomas, R.; MacKenzie, A.; Brownlow, R.; Lowry, D.; Fisher, R.; Nisbet, E. Atmospheric Sampling on Ascension Island Using Multirotor UAVs. *Sensors* **2017**, *17*, 1189, doi:10.3390/s17061189.
9. Chang, C.-C.; Chang, C.-C.; Wang, J.-L.; Chang, C.-Y.; Chang, C.-Y.; Liang, M.-C.; Lin, M.-R. Development of a Multicopter-Carried Whole Air Sampling Apparatus and Its Applications in Environmental Studies. *Chemosphere* **2015**, *144*, 484-492, doi:10.1016/j.chemosphere.2015.08.028.
10. Allen, G.; Hollingsworth, P.; Kabbabe, K.; Pitt, J.R.; Mead, M.I.; Illingworth, S.; Roberts, G.; Bourn, M.; Shallcross, D.E.; Percival, C.J. The Development and Trial of an Unmanned Aerial System for the Measurement of Methane Flux from Landfill and Greenhouse Gas Emission Hotspots. *Waste Management* **2018**, *87*, 883-892, doi:10.1016/j.wasman.2017.12.024.

 doi:10.20944/preprints202603.1924.v1

11. Fosco, D.; De Molfetta, M.; Renzulli, P.; Notarnicola, B. Progress in Monitoring Methane Emissions from Landfills Using Drones: An Overview of the Last Ten Years. *The Science Of The Total Environment* **2024**, *945*, 173981, doi:10.1016/j.scitotenv.2024.173981.
12. Tanda, G.; Balsi, M.; Fallavollita, P.; Chiarabini, V. A UAV-Based Thermal-Imaging Approach for the Monitoring of Urban Landfills. *Inventions* **2020**, *5*, 55, doi:10.3390/inventions5040055.
13. Gaceta Del Gobierno Del Estado de México. (2009). Decreto 293.- Convenio de Asociación Municipal Para La Operación de Un Relleno Sanitario Regional, y Se Aprueba La Creación de Un Organismo Público Descentralizado Encargado de La Operación Del Relleno Sanitario Regional.
14. Espejel, R. Juchitepec cuenta con un relleno sanitario de primer nivel: Mejía - El Valle Available online: https://elvalle.com.mx/2020/01/30/juchitepec-cuenta-con-un-relleno-sanitario-de-primer-nivel-mejia/.
15. Secretaría de Medio Ambiente y Recursos Naturales; Trujillo Segura, J.C.J.; Ortiz Conde, R.; Medina Arévalo, A.; Acevedo Portilla, L.F.; Navarro Reynoso, J.E.; Alcantar López, G.; Mendoza Aguirre, S.I.; Trigueros Esquiliano, R.; Díaz Ortiz, M.; et al. *Diagnóstico Básico Para La Gestión Integral de Los Residuos*; Primera.; 2020;
16. Bailey, S.C.C.; Sama, M.P.; Canter, C.A.; Pampolini, L.F.; Lippay, Z.S.; Schuyler, T.J.; Hamilton, J.D.; MacPhee, S.B.; Rowe, I.S.; Sanders, C.D.; et al. University of Kentucky Measurements of Wind, Temperature, Pressure and Humidity in Support of LAPSE-RATE Using Multisite Fixed-Wing and Rotorcraft Unmanned Aerial Systems. *Earth System Science Data* **2020**, *12*, 1759-1773, doi:10.5194/essd-12-1759-2020.
17. De Boer, G.; Palo, S.; Argrow, B.; LoDolce, G.; Mack, J.; Gao, R.-S.; Telg, H.; Trussel, C.; Fromm, J.; Long, C.N.; et al. The Pilatus Unmanned Aircraft System for Lower Atmospheric Research. *Atmospheric Measurement Techniques* **2016**, *9*, 1845-1857, doi:10.5194/amt-9-1845-2016.
18. Emran, B.; Tannant, D.; Najjaran, H. Low-Altitude Aerial Methane Concentration Mapping. *Remote Sensing* **2017**, *9*, 823, doi:10.3390/rs9080823.
19. Baiocchi, V.; Napoleoni, Q.; Tesei, M.; Servodio, G.; Alicandro, M.; Costantino, D. UAV for Monitoring the Settlement of a Landfill. *European Journal Of Remote Sensing* **2019**, *52*, 41-52, doi:10.1080/22797254.2019.1683471.
20. Khan, A.; Schaefer, D.; Tao, L.; Miller, D.J.; Sun, K.; Zondlo, M.A.; Harrison, W.A.; Roscoe, B.; Lary, D.J. Low Power Greenhouse Gas Sensors for Unmanned Aerial Vehicles. *Remote Sensing* **2012**, *4*, 1355-1368, doi:10.3390/rs4051355.
21. De Sousa Mello, C.C.; Salim, D.H.C.; Simões, G.F. UAV-Based Landfill Operation Monitoring: A Year of Volume and Topographic Measurements. *Waste Management* **2021**, *137*, 253-263, doi:10.1016/j.wasman.2021.11.020.
22. Alejo-Sanchez, L.E.; Márquez-Grajales, A.; Salas-Martínez, F.; Franco-Arcega, A.; López-Morales, V.; Acevedo-Sandoval, O.A.; González-Ramírez, C.A.; Villegas-Vega, R. Missing Data Imputation of Climate Time Series: A Review. *MethodsX* **2025**, *15*, 103455, doi:10.1016/j.mex.2025.103455.
23. AlSalehy, A.S.; Bailey, M. Improving Time Series Data Quality: Identifying Outliers and Handling Missing Values in a Multilocation Gas and Weather Dataset. *Smart Cities* **2025**, *8*, 82, doi:10.3390/smartcities8030082.
24. Oliver, M.A.; Webster, R. A Tutorial Guide to Geostatistics: Computing and Modelling Variograms and Kriging. *CATENA* **2013**, *113*, 56-69, doi:10.1016/j.catena.2013.09.006.
25. Munyati, C.; Sinthumule, N.I. Comparative Suitability of Ordinary Kriging and Inverse Distance Weighted Interpolation for Indicating Intactness Gradients on Threatened Savannah Woodland and Forest Stands. *Environmental And Sustainability Indicators* **2021**, *12*, 100151, doi:10.1016/j.indic.2021.100151.
26. Alsamamra, H.; Ruiz-Arias, J.A.; Pozo-Vázquez, D.; Tovar-Pescador, J. A Comparative Study of Ordinary and Residual Kriging Techniques for Mapping Global Solar Radiation over Southern Spain. *Agricultural And Forest Meteorology* **2009**, *149*, 1343-1357, doi:10.1016/j.agrformet.2009.03.005.
27. Tanda, G.; Balsi, M.; Fallavollita, P.; Chiarabini, V. A UAV-Based Thermal-Imaging Approach for the Monitoring of Urban Landfills. *Inventions* **2020**, *5*, 55, doi:10.3390/inventions5040055.
28. Sledz, A.; Unger, J.; Heipke, C. THERMAL IR IMAGING: IMAGE QUALITY AND ORTHOPHOTO GENERATION. *1* **2018**, doi:10.5194/isprs-archives-XLII-1-413-2018.

 doi:10.20944/preprints202603.1924.v1

29. Kelly, J.; Kljun, N.; Olsson, P.-O.; Mihai, L.; Liljeblad, B.; Weslien, P.; Klemedtsson, L.; Eklundh, L. Challenges and Best Practices for Deriving Temperature Data from an Uncalibrated UAV Thermal Infrared Camera. *Remote Sensing* **2019**, *11*, 567, doi:10.3390/rs11050567.
30. Kostrzewa, A.; Płatek-Żak, A.; Banat, P.; Wilk, Ł. Open-Source vs. Commercial Photogrammetry: Comparing Accuracy and Efficiency of OpenDroneMap and Agisoft Metashape. *The International Archives of the Photogrammetry, Remote Sensing and Spatial Information Sciences/International Archives of the Photogrammetry, Remote Sensing and Spatial Information Sciences* **2025**, *XLVIII-1/W4-2025*, 65–72, doi:10.5194/isprs-archives-xlviii-1-w4-2025-65-2025.
31. Brovkina, O.; Fajmon, L.; Pikl, M.; Zemek, F. Application of UAV Orthophoto and Thermal Imaging for Municipal Solid Waste Landfills Monitoring. *ISPRS Annals Of The Photogrammetry, Remote Sensing And Spatial Information Sciences* **2025**, *X-2/W2-2025*, 1-6, doi:10.5194/isprs-annals-x-2-w2-2025-1-2025.